Structural Evolution of Phosphated Alumina during Sol−Gel Synthesis

Enrique Lima,*,† Jaime Valente,‡ Pedro Bosch,§ and Victor Lara†

Universidad Autónoma Metropolitana, Iztapalapa, Avenida San Rafael Atlixco No. 186,
A. P. 55-532, 09340 México D.F., Mexico, Instituto Mexicano del Petróleo, Eje Central L. Cárdenas 152,
A. P. 14-805, 07730 México D.F., Mexico, and Instituto de Investigaciones en Materiales, UNAM,
Circuito Exterior, A. P. 70-360, 04510 México D.F., Mexico

Phosphated alumina gels were prepared by the sol−gel method. Gels were aged from 1 to 8 days in air. Gel structure evolution, as time went on, was followed by ^{27}Al magic angle spinning nuclear magnetic resonance, X-ray diffraction, and small-angle X-ray scattering. It is concluded that the aging time is a crucial parameter in the formation of coordinately unsaturated sites of aluminum (Al^{IV} and Al^{V}). The gel network is shown to have a fractal structure.

Introduction

Aluminas have been widely studied due to their use as ceramics and as catalysts (and catalyst supports) in petrochemistry since alumina adds a dual functionality to the catalyst.[1] Indeed, the purpose is to convert low-octane components to high-octane isoparaffins. This function is fulfilled by the supported metal, and the acidic function of the support accomplishes the isomerization and cyclization of normal paraffins. Many strategies have been proposed to modify the alumina surface properties. In this sense, the introduction of lanthana or ceria, among other oxides, has provided solids with improved acidity.[2] Furthermore, the modifications may be structural. Through theoretical studies, the formation of surface perovskite has been proposed in the system La$_2$O$_3$/γ-Al$_2$O$_3$.[3]

γ-Alumina is the preferred support for hydrodesulfurization catalysts (since it provides a good dispersion of the active sites) such as MoS$_2$ or WS$_2$ promoted by cobalt or nickel.[4] Commonly, these supports are prepared by precipitation and calcination of aluminum oxyhydroxides. Therefore, mesoporous solids having a high surface area ($\geq$250 m^2/g) and a narrow pore size distribution are highly desired. In this system, phosphorus is often used to inhibit acidity and also to promote the dispersion of the active phases, although the role of phosphorus is not yet fully understood.[5]

Sol−gel preparation has been found to provide an accurate control of the structural and textural properties; i.e., more homogeneous materials with a high specific surface area are obtained.[6,7] The control of aging time is important for obtaining the required material. Nevertheless, the synthesis mechanism is not well established because the used characterization techniques are limited either by the experimental requirements or by conventional concepts. These materials are, indeed, microcrystalline and heterogeneous. The gels are even more complex as translational symmetry does not predict the spatial relationship between atoms in these structures. In this sense, fractal geometry offers a rather new and enriching option. Usually, sample features are described in terms of Euclidean

geometry: flat planes, perfect spheres, or ideal pyramids. Fractal geometry extends the study of natural complexity, e.g., heterogeneous processes as sol−gel synthesis that are highly sensitive to geometric details.

Materials such as SiO$_2$ aerogels and TiO$_2$ have been successfully characterized through fractal geometry using the small-angle X-ray scattering (SAXS) technique.[8−10] In Co-exchanged X zeolites, the fractal dimension has been correlated to cobalt leaching. Recently, SAXS characterization has been performed on aluminum-containing gels to show that the network is built up from small aggregates and it is not fractal.[11] The aim of the present work is to follow the effect of aging time on particle shape and structure in a phosphated alumina gel. The system is closed, but for comparison purposes a gel exposed to air is also presented. Geometry is described in terms of fractal dimension, whereas structure is described in terms of radial distribution functions, obtained in conditions as similar as possible to in situ experiments. Also, the coordination of aluminum ions is stated by solid-state nuclear magnetic resonance.

Experimental Section

Samples. Gel samples were prepared as follows: aluminum tri-*sec*-butoxide (ATB) was dissolved and refluxed at 80 °C in absolute anhydrous ethyl alcohol (EtOH) for 1 h. Then, hydrolysis was catalyzed by a 3 N phosphoric acid solution added slowly and refluxing for 1 h. The system was cooled to room temperature, allowing the hydrolysis to complete and form a gel. The molar ratios of the reactants were EtOH:ATB = 60: 1, H$_3$PO$_4$:ATB = 0.03:1, and H$_2$O:ATB = 1:1. All the gel was placed in an open glass vessel and aged for several days in air at room temperature.

Gel samples were not calcined; they were taken from the reaction recipient at time intervals of 1, 2, 3, and 8 days. Samples were labeled as G1, G2, G3, and G8, respectively. G8 was characterized as wet gel and also as dried gel (at 80 °C). The samples were studied by SAXS, XRD, and NMR.

Powder X-ray Diffraction (XRD). A molybdenum wavelength was used to reach the high values of the *h* parameter ($h = 4\pi \sin \theta/\lambda$) required to obtain the radial distribution functions. The Kα radiation was selected with a filter, and the data, measured by step scanning with a scintillation counter, were the input to the Radiale program.[12] An adapted sample holder which was able to contain some drops of wet sample was used.

* Corresponding author. Phone: (525) 58044667. Fax: (525) 58044666. E-mail: lima@xanum.uam.mx.
† Universidad Autónoma Metropolitana.
‡ Instituto Mexicano del Petróleo.
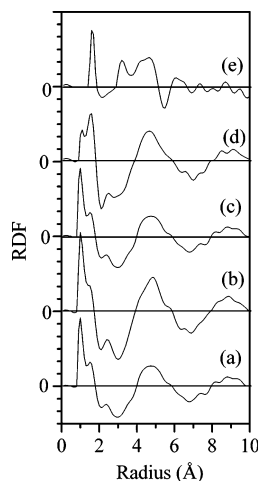§ Instituto de Investigaciones en Materiales, UNAM.

Figure 1. Radial distribution functions of gel samples (a, b, c, and d correspond to G1, G2, G3, and G8, respectively) compared to dried G8 material (e).

Then the data were collected from the evolving sample in air at room temperature.

NMR Spectroscopy. [27]Al spectra were obtained in the solid state in a static field of 7.05 T (ASX-300 Bruker spectrometer), under magic angle spinning (MAS) conditions. The spinning rate was 10 kHz. The one-pulse spectra were obtained with a $\pi/2$ pulse length of 2 μs; the delay between pulses was 0.5 s. A high-resolution MAS probe was used in a DMX-500 Bruker spectrometer. Although samples were introduced as gels, they were slightly dried before the NMR measurements, due to the spinning. Spectra correspond, therefore, to gel samples slightly dried at room temperature.

Small-Angle X-ray Scattering (SAXS). A Kratky camera coupled to a copper anode tube was used to measure the SAXS curves. The distance between the sample and the linear proportional counter was 25 cm; a Ni filter selected the copper Kα radiation. The sample was introduced into a capillary tube. Intensity $I(h)$ was measured for 9 min to obtain good-quality statistics.

The SAXS data were processed with the ITP program,[13-17] where the angular parameter (h) is defined as $h = [4\pi \sin(\theta/2)]/\lambda$; θ and λ are the X-ray scattering angle and the wavelength, respectively. The radius of gyration (R_g) could, then, be obtained from the slope of the Guinier plot, log $I(h)$ versus h^2,[18] in the zone 1×10^{-3} Å^{-2} < h^2 < 7×10^{-3} Å^{-2}.

The shape of the scattering objects was estimated from the Kratky plot, i.e., $h^2[I(h)]$ versus h. If the curve presents a peak, the particles are globular (bubbles).[19] If a shape can be assumed,[15] the size distribution function may be calculated.

Finally, from the slope of the curve log $I(h)$ vs log h, the fractal dimension of the scattering objects[20,21] was determined. For this study the background obtained with the Porod plot was subtracted from the experimental intensity. The h interval was $0.07 < h < 0.18$ Å^{-1}.

Note that, by the Babinet principle, the small-angle X-ray scattering may be due either to dense particles in a low-density environment or to pores—or low-density inclusions—in a continuous high electron density medium.

Results

X-ray Diffraction. The radial distribution functions of the gel samples are compared in Figure 1 from G1 to the dried G8 powder. The radial distribution functions of the gels are all similar; they only differ in the relative size of the first and second peaks. The first peak, located at 1.1 Å, corresponds to organic bonds (C—H and O—H) due to the presence of ethanol, and
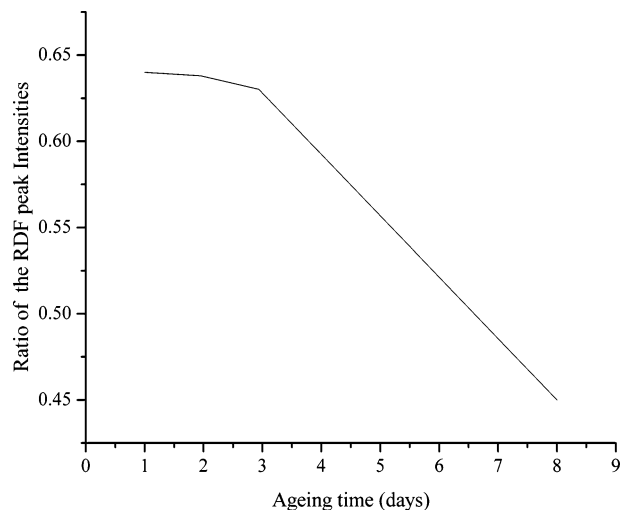

Figure 2. Ratio of r = 1.1 Å and (1.1 + 1.7) Å peak intensities of radial distribution functions presented in Figure 1 as a function of aging time.
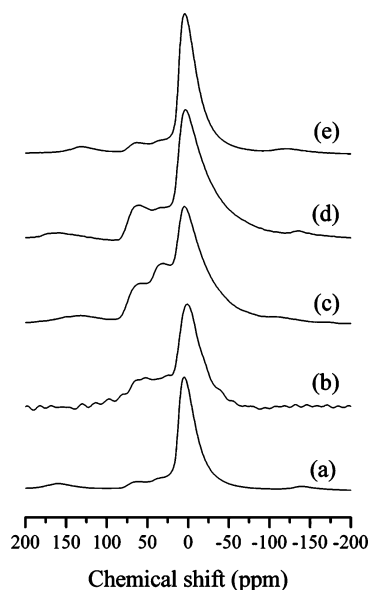

Figure 3. ^{27}Al MAS NMR spectra of gel samples: (a) G1; (b) G2; (c) G3; (d) G8; (e) dried G8.

the second at 1.7 Å may be attributed to an Al—O bond. The first peak, compared to the second, diminishes as time goes on. To quantify such an evolution, the ratio of the first peak to the sum of the first and the second peak intensities was calculated. Thus, as the organic bonds disappear due to the evaporation of the alcohol the aluminum oxygen bonds are formed; see Figure 2. As a plateau is observed up to 72 h (G3), the organic materials start to evaporate only at longer times. An aging time may be then defined to favor the formation of Al—O—Al bonds: it is the time elapsed to reach the knee observed in Figure 2. The third peak, at 2.6 Å, may be attributed to the chain C—C—H from the ethanol. As expected, this peak is very low in the wet 8 days gel (G8), and it is not present in the corresponding dried material. In this trend, the diffraction pattern of the dried G8 is very representative as it corresponds only to boehmite; the structure of the final material is indeed well-defined and identified.

^{27}Al NMR Spectroscopy. Figure 3 displays the ^{27}Al MAS NMR spectra for the gel series. In the spectrum corresponding to the 1 day aged gel, a high-intensity peak at 4 ppm, due to octahedrally coordinated aluminum (Al[VI]), is observed; the small

Structural Evolution of Phosphated Alumina Gels

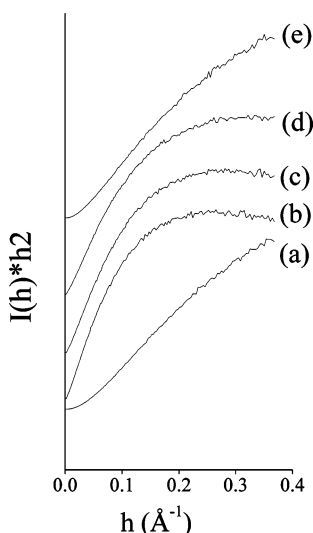*J. Phys. Chem. B, Vol. 109, No. 37, 2005* **17437**

Figure 4. Kratky plots of samples: (a) G1; (b) G2; (c) G3; (d) G8; (e) dried G8. The shape of the G1 curve corresponds to fibers; the curves for G2, G3, and G8 gel samples are typical of platelets.
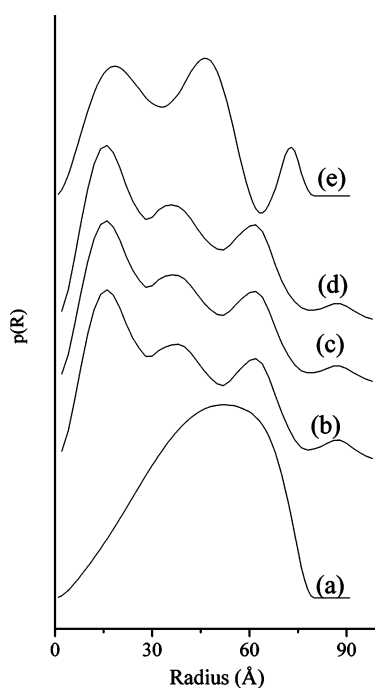

Figure 6. Log $I(h)$ versus log h plots to obtain the fractal dimension.

Figure 5. Particle size distributions in (a) G1, (b) G2, (c) G3, (d) G8, and (e) dried G8.

Figure 7. Fractal dimension (—) and relative amount of CUS aluminum (---) as a function of gel aging time. *Ratio $(Al^{IV} + Al^{V})/(Al^{IV} + Al^{V} + Al^{VI})$ calculated from the corresponding ^{27}Al NMR signal intensities.

peaks at 32 and 60 ppm are due to pentahedral (Al^{V}) and tetrahedral (Al^{IV}) aluminum species, respectively.[22,23] In the gel samples G2 and G3, the relative amount of Al^{V} and Al^{IV} increases, in contrast to the sample aged for 8 days, wet G8, where the amount of these species decreased. The dried gel G8, if compared to the wet corresponding sample, does not exhibit, strictly, the same relative amount, and these species slightly diminish.

Small-Angle X-ray Scattering. When the gel samples were characterized by small-angle X-ray diffraction, the shape of the scattering objects evolved from fibers (sample G1) to platelets (G2, G3, and G8) as shown by the Kratky plots; see Figure 4. The scattering objects in SAXS may be either high or low electron density zones. In this study the samples do not present any porosity or bubbles; hence the scattering must be due to particles or inhomogeneities present in the gel, most probably agglomerations of primary structural units. In the G1 sample
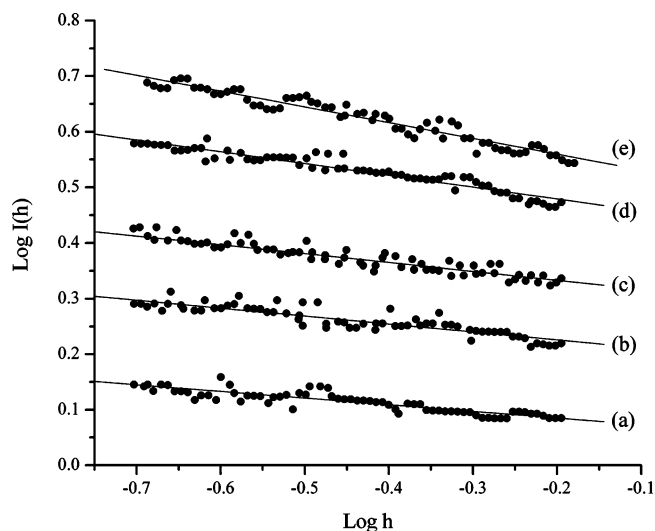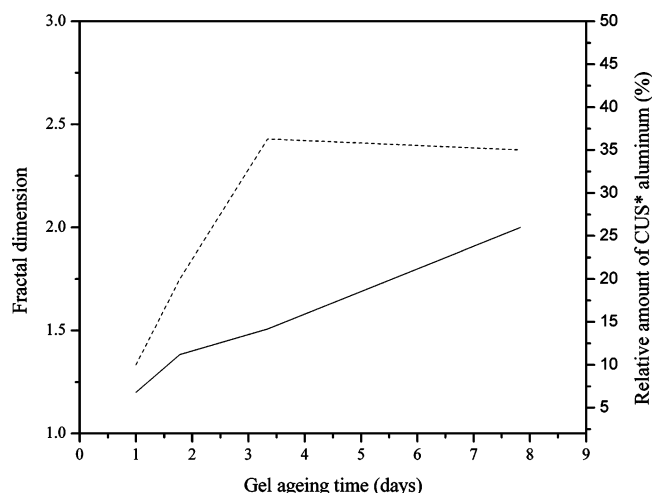
these structural units are associated as a linear polymer, which with time cross-link to constitute small platelets.

Assuming such shapes, the particle size distributions were calculated; see Figure 5. The size distribution of sample G1 is monomodal and presents a maximum at 50 Å, but as the peak is very broad, it has to be concluded that the radius of the chains is comprised between 30 and 70 Å. The other three samples present a half-thickness of the platelets of 18 Å which corresponds to the main peak of the distribution. Two more peaks are found at 37 and 60 Å, showing that the distribution is not homogeneous.

It is not possible to determine by SAXS the contribution of each particle size to the fractal dimension or the electron density profile. The following data, then, correspond to a representative average of the materials. The fractal dimension of the samples was obtained from the slope of log $I(h)$ versus log h in the zone $-0.68 < \log h < -0.40$; see Figure 6. The obtained values were 1.2 for sample G1, 1.4 and 1.5 for samples G2 and G3, and 2.0 for the wet G8 sample. The G8 dried sample presented a fractal dimension of 2.2. Although samples G2, G3, and G8 are similar, as far as their shapes and their particle size distributions are concerned, they can be distinguished through their fractal dimension; see Figure 7. A clear correlation between time and fractal dimension exists: The fractal dimension in-
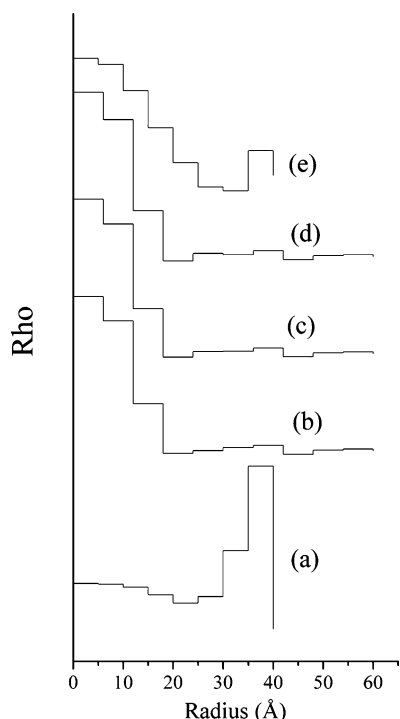
Figure 8. Electron density profiles of samples: (a) G1; (b) G2; (c) G3; (d) G8; (e) dried G8.

creases linearly as time goes on. However, the wet and dried 8 days gel (G8) are almost the same. Of course, fractal dimension is a morphological parameter and it does not reflect the structural evolution given by the NMR and X-ray diffraction results. In Figure 7 the relative amount of coordinated unsaturated sites (CUS) of aluminum, i.e., Al^{IV} and Al^{V}, is presented, as a function of time and compared to fractal dimensions. Note that the amount of CUS increases linearly with time up to 3 days. For aging times greater than 3 days a slight diminution is observed.

The electron density profiles, presented in Figure 8, correspond again to the averaged samples. They do not reflect the particle size distributions. However, they represent a general tendency. In the initial gel (1 day aged), only sharp changes of electron density are observed and the center of the scattering objects is constituted by a low-density material, most probably the solvent. In the materials aged more than 1 day (2 up to 8 days), a smooth transition from the high-density component to the low-density component is observed.

Discussion

Structure. As the organic solvent present in the gel disappears, the Al–O–Al bonds are formed after an aging time of 72 h as shown by X-ray diffraction. However, by NMR we found that gels are already reacting since the first 24 h.

A gel aged for 1 day contains a high percentage of aluminum in octahedral coordination; i.e., polycations such as $[Al(H_2O)_6]^{3+}$, $[Al_2(OH)_2(H_2O)_8]^{4+}$, and $[AlO_4Al_{12}(OH)_{24}(H_2O)_{12}]^{7+}$ are formed.[24,25] In samples aged for 2 or 3 days, the relative amount of coordinated unsaturated sites (CUS) of aluminum increases. The general trend is that the number of ligands per aluminum decreases as solvent evaporates.
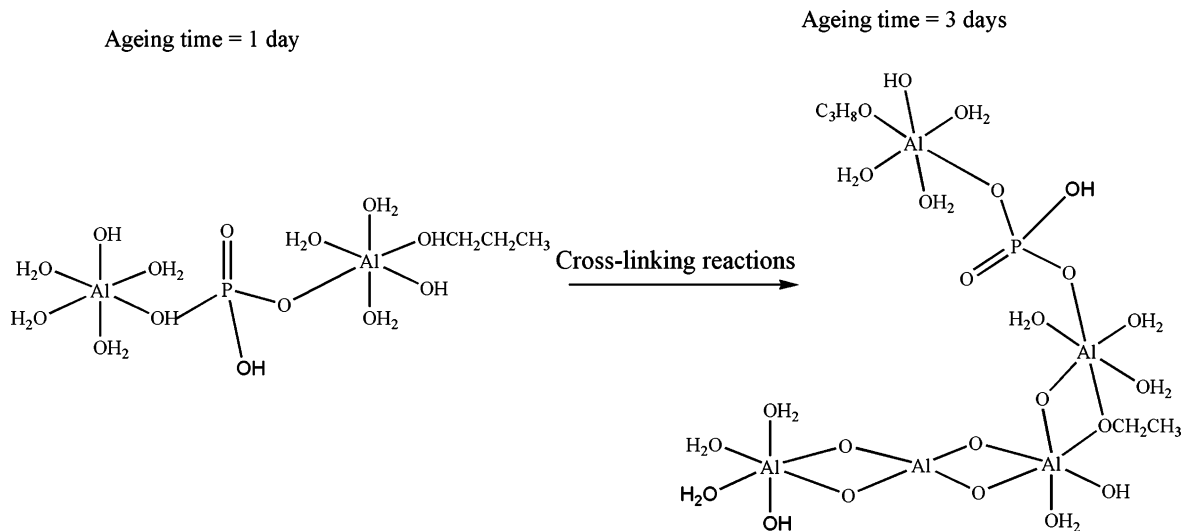

Figure 9. Representation of the aluminum octahedral bridged by the phosphorus species and its evolution as the phosphated alumina gel is aged.
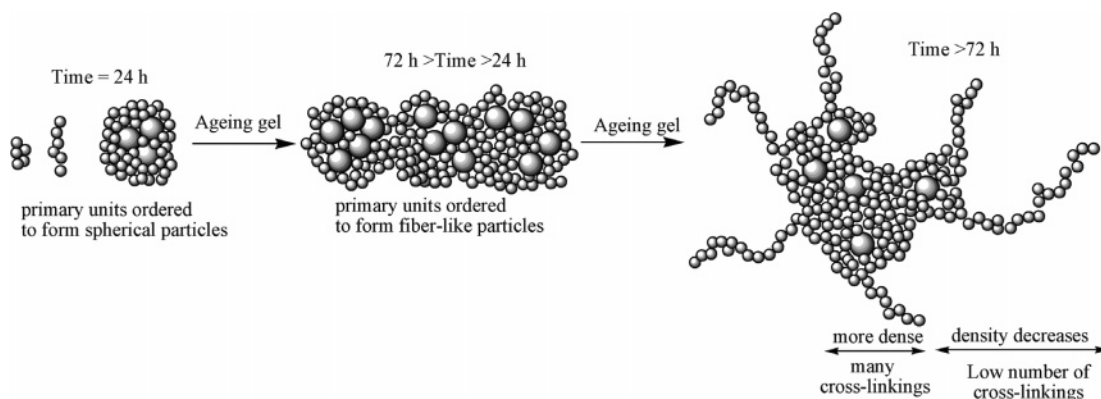

Figure 10. Model showing evolution of aggregates of primary units (•) and solvent (●) as time goes on during synthesis of phosphated alumina.

Structural Evolution of Phosphated Alumina Gels

J. Phys. Chem. B, Vol. 109, No. 37, 2005 **17439**

These results, apparently contradictory, are complementary. Since the first 24 h the gel reacts to link the building units, i.e., the polycations already mentioned. Up to 72 h, these polycations are fairly large units and the short-range order, i.e., the interatomic first- and second-neighbor distances, is maintained. Then, differences in the diffraction patterns and, thus, in the radial distribution functions are minimal. In fact, the presented radial distribution functions were calculated only up to a radius of 10 Å. The evolution in the ordering of the sample must be visible at larger radial distances where the radial distribution function is not very precise. The new ordering must be due to cross-linking. This hypothesis is based on the NMR results: With solvent evaporation the number of ligands per aluminum decreases; aluminum chains, then, are cross-linked generating CUS aluminum.

In the gel aged for 8 days, the relative amount of CUS aluminum diminishes. The gel is almost dried and transformed to crystalline boehmite, where the aluminum atoms are octahedrally coordinated. Such a difference, in the short-range order, is clearly revealed by the corresponding radial distribution function.

The following model, then, emerges at a molecular level. Building units, constituted by aluminum polycations, are immersed in the solvent; they are free to diffuse. As solvent and water evaporate, the concentration of polycations increases; they interact to form aggregates as shown by the formation of CUS aluminum atoms, although the average short-range order is not altered. Of course, time, temperature, and concentration individually contribute to direct the crystallization as they do in the aluminophosphate molecular sieve synthesis.

The P–O distance is 1.54 Å, and it is not observed in our radial distribution functions. If such a distance was present, it would be clearly resolved because the first peak was found at $r = 1.1$ Å and the second at $r = 1.7$ Å. However, the phosphorus amount is very small, and even if its influence on crystallization is crucial, it cannot be detected by X-ray diffraction. It seems that phosphorus is the bridge to link aluminum primary building units; see Figure 9.

Morphology. Structural changes determine the morphological modifications observed by SAXS. The shape of the initial agglomerates of aluminum is linear (G1 sample), and after 48 h it turns out to be plateletlike. The polycations are known to be spherical; then in the G1 sample these spheres unite to constitute a necklace-shaped fiber. As solvent and water evaporate, these fibers densify and cross-link, constituting sieves that appear to SAXS as platelets, but the initial atomic structure is not altered.

These considerations are in agreement with the aluminum coordination found by NMR. In this sense, fractal dimension, understood as the connectivity of the platelets, is most illustrative. It reveals how the network is densified and ordered with aging time. The half-thickness of such platelets is only 18 Å, whereas all the initial filaments had a radius of 50 Å. In the flakelike platelets, constituted by the agglomeration of linear assemblies of polycations, the core is denser than the external zone. The correlation between the fractal dimension and the relative amount of CUS aluminum shows again that densification is due to cross-linking.

From SAXS curves the average electron density may be estimated. As with fractal dimension, these are average, and hence their interpretation, in a polydisperse system as ours, is not straightforward. Nevertheless, they show a trend. The first sample points to the following model: the large building units, the spherical pearls of the necklace, are constituted by a low-density core surrounded by an aluminum polymer. The platelet density diminishes with distance; hence the amount of cross-linking diminishes. Figure 10 illustrates such a model.

Conclusion

Under the synthesis conditions used in this work, the Al^{3+} ions build up a gel network that initially contains spherically shaped primary units (polycations). As the gel is aged, the primary units aggregate to form particles that evolve from fiberlike to platelets. Such a mechanism can be described with fractal dimension; the fractal dimension increases linearly with time. Coordinated unsaturated sites of aluminum are created preferentially when gel is aged for 3 days.

References and Notes

(1) Richardson, J. T. Principles of Catalyst Development. In *Fundamental and Applied Catalysis*; Twigg, M. V., Spencer, M. S., Eds.; Plenum Press: New York, 1989; pp 23−39.

(2) Shaper, H.; Doesburg, E. B. M.; Van Reijen, L. *Appl. Catal.* **1983**, *7*, 211.

(3) Alvarez, L. J.; Fernández, J.; Capitán, M. J.; Odriozola, J. A. *Catal. Lett.* **1993**, *21*, 89.

(4) Grimblot, J. *Catal. Today* **1998**, *41*, 111.

(5) Iwamoto, R.; Grimblot, J. *J. Catal.* **1999**, *44*, 417.

(6) Coster, D.; Fripiat, J. *Chem. Mater.* **1993**, *5*, 1204.

(7) Sánchez-Valente, J.; Bokhimi, X.; Hernández, F. *Langmuir* **2003**, *19*, 3583.

(8) Dieudonné, Ph.; Phalippou, J. *J. Sol-Gel Sci. Technol.* **1999**, *14*, 249.

(9) Hackley, V. A.; Anderson, M. A.; Spooner, S. *J. Mater. Res.* **1992**, *7*, 2555.

(10) Lima, E.; Bosch, P.; Lara, V.; Bulbulian, S. *Chem. Mater.* **2004**, *16*, 2255.

(11) Sinkó, K.; Mezei, R.; Rohonczy, J.; Fratzl, P. *Langmuir* **1999**, *15*, 6631.

(12) Magini, M.; Cabrini, A. *J. Appl. Crystallogr.* **1972**, *29*, 702.

(13) Glatter, O. *J. Appl. Crystallogr.* **1981**, *14*, 101.

(14) Glatter, O. *J. Appl. Crystallogr.* **1988**, *21*, 886.

(15) Glatter, O. *Science* **1991**, *84*, 46.

(16) Glatter, O.; Hainisch, B. *J. Appl. Crystallogr.* **1984**, *17*, 435.

(17) Glatter, O.; Gruber, K. *J. Appl. Crystallogr.* **1993**, *26*, 512.

(18) Guinier, A.; Fournet, G. *Small-Angle Scattering of X-rays*; John Wiley & Sons: New York, 1955.

(19) Kataoka, M.; Flanagan, J. M.; Tokunaga, F.; Engelman, D. M. Use of X-ray solution scattering for protein folding study. In *Synchrotron Radiation in the Biosciences*; Chanse, B., Deisenhofer, J., Ebashi, S., Goodhead, D. T., Huxley, H. E., Eds.; Clarendon Press: Oxford, UK, 1994; pp 87−92.

(20) Harrison. A. *Fractals in Chemistry*; Oxford University Press: New York, 1995.

(21) Martin, J. E.; Hurd, A. J. *J. Appl. Crystallogr.* **1987**, *20*, 61.

(22) Lippmaa, E.; Samoson, A.; Mägi, M. *J. Am. Chem. Soc.* **1986**, *108*, 1730.

(23) Coster, D.; Blumenfeld, A. L.; Fripiat, J. *J. Phys. Chem.* **1994**, *98*, 6201.

(24) Kloprogge, J. T.; Seykens, D.; Geus, J. W.; Jansen, J. B. *J. Non-Cryst. Solids* **1993**, *160*, 144.

(25) Bottero, J. Y.; Tchoubar, D.; Cases, J. M.; Fiessinger, F. *J. Phys. Chem.* **1982**, *86*, 3667.